Available online at www.sciencedirect.com
SCIENCE DIRECT®
Journal of Molecular Structure 649 (2003) 143–153
Journal of MOLECULAR STRUCTURE
www.elsevier.com/locate/molstruc

Low temperature polymorphism in 3-amino-1-propanol

C. Cacela[a,b], A. Baudot[c], M.L. Duarte[a], A.M. Matos-Beja[d], M. Ramos Silva[d], J.A. Paixão[d], R. Fausto[b,*]

[a]*Departamento de Química e Bioquímica, CECUL, Faculdade de Ciências, Universidade de Lisboa, Portugal*
[b]*Centro de Química de Coimbra, Departamento de Química, Universidade de Coimbra, Coimbra 3004-535, Portugal*
[c]*Centre de Recherches sur les Trés Basses Températures (CNRS),Grenoble, France*
[d]*Centro de Estudos de Materiais por Difracção de Raios-X, Departamento de Física, Universidade de Coimbra, Portugal*

Received 14 November 2002; revised 6 January 2003; accepted 6 January 2003

Abstract

3-Amino-1-propanol (**3AP**) was investigated by differential scanning calorimetry, and low temperature powder X-ray diffraction and Raman spectroscopy. Within the range of temperatures studied (− 150–25 °C), **3AP** was found to be able to crystallize in two monotropic polymorphs. Fast cooling rates produce an amorphous state that, on heating, crystallizes into the metastable polymorph. At higher temperatures, this metastable crystalline phase converts into the stable crystal. Using intermediate cooling rates, **3AP** crystallizes as the metastable polymorph, the solid ⇛ solid transition leading to conversion of this form into the stable polymorph occurring during the subsequent heating. Slower cooling rates enable formation of the stable crystal on cooling. The two crystalline polymorphs were structurally characterized by powder X-ray diffraction and Raman spectroscopy. It was concluded that different conformations are assumed by the individual molecules of **3AP** in the two crystalline varieties, with the molecules assuming the all-*trans* configuration in the metastable crystalline state and having the heavy atom backbone *trans* but the NH_2 and OH groups *gauche* in the stable crystal.

Keywords: 3-Amino-1-propanol; X-ray diffraction and Raman spectroscopy; Differential Scanning Calorimetry

1. Introduction

Simple amino-alcohols with short carbon chains can be used as ice crystallization inhibitors, thus having a potential application in cryobiology as cryoprotectant agents for vitrification of biological material [1]. In a series of previous publications [2–5], we report the results of a systematic study on the physicochemistry of four linear amino-alcohols—2-amino-1-ethanol (**2AE**), *R*-2-amino-1-propanol (**2AP**), *R*-1-amino-2-propanol (**1AP**) and 3-amino-1-propanol (**3AP**)—in both the liquid and gaseous phases as well as isolated in low temperature inert gas matrixes.

For the matrix-isolated molecules, as well as in the gaseous phase, the most populated conformational states of all the studied amino-alcohols were found to be folded structures bearing an intramolecular OH···N hydrogen bond. In their more stable conformations all the studied molecules assume a *gauche*

* Corresponding author. Tel.: +351-239-827-703; fax: +351-239-852-080.
E-mail address: rfausto@ci.uc.pt (R. Fausto).

0022-2860/03/$ - see front matter © 2003 Elsevier Science B.V. All rights reserved.
doi:10.1016/S0022-2860(03)00049-8

configuration of the OCCN axis (or NCCC and CCCO in the case of **3AP**), which provides a better spatial arrangement of the OH and NH_2 groups for the establishment of the OH···N intramolecular hydrogen bond. For **3AP**, the population of the most stable conformer (conformer **g′GG′g**, shown in Fig. 1) was found to be larger than 90%, both in gas phase and for the matrix-isolated compound [3,6–8]. The strength of the OH···N intramolecular hydrogen bond in this conformer was estimated to be ≈ 21 kJ mol^{-1} [6].

In the condensed phases, pronounced changes on the relative importance of the different monomeric species were expected to occur, since in these phases a new set of possible interactions, including relatively strong intermolecular hydrogen-bond interactions, can operate. Indeed, in the liquid phase of all the previously studied amino-alcohols OH···N intermolecular hydrogen bonding is strongly predominant, leading to extensive disruption of the OH···N intramolecular interaction [2–6]. On the other hand, the NH···O intramolecular interaction gains further importance, since this interaction activates both the OH group to act as hydrogen donor and the nitrogen atom to act as hydrogen acceptor, thus leading to stronger intermolecular OH···N bonds [2–6]. For **3AP**, the preferred structure of the monomeric unit within the aggregates in the liquid phase was found to be similar to conformer **g′G′Gg** in (Fig. 1), which corresponds to the third more stable conformer in the gas phase [3,6]. Very interestingly, in contrast with the results obtained for **2AE**, **2AP** and **1AP**, for **3AP** it was still possible to detect some free molecules in the liquid; these molecules adopt a configuration similar to the **3AP** gas-phase conformational ground state (conformer **g′GG′g**; see Fig. 1), in consonance with the stronger intramolecular OH···N bond in **3AP** when compared with the same interaction in the remaining three studied amino-alcohols [2–6].

After having studied the isolated molecule and the liquid phase of the above mentioned amino-alcohols, investigation of their solid phases appeared as a natural continuation of our studies, even more since a transition from the liquid to solid state is very often accompanied by important changes in the structure of the individual molecules. In a disordered liquid, a mixture of different molecular conformations is in general observed, while in a crystal most of times the molecules assume a unique conformation. Moreover, a change in the conformation of individual molecules in the solid state is usually accompanied by a change in the crystalline structure itself, i.e. it defines a different polymorph [9–11].

In this paper, we present the results concerning the solid state of **3AP**, investigated by differential scanning calorimetry (DSC), and low temperature powder X-ray diffraction and Raman spectroscopy.

2. Experimental

3-Amino-1-propanol was obtained spectroscopic grade from Aldrich (purity 99 + %). Since

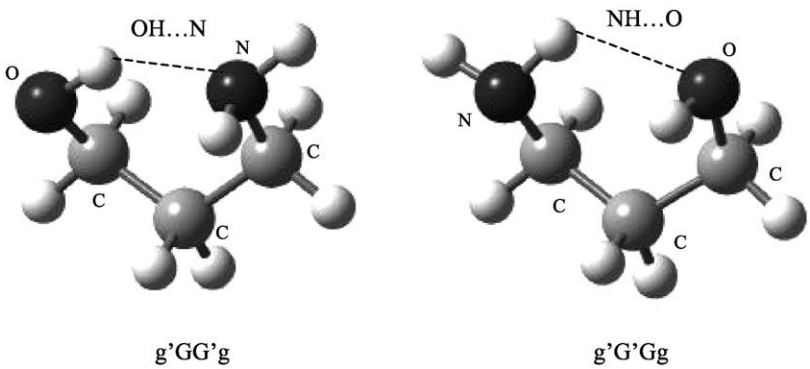

g'GG'g g'G'Gg

Fig. 1. The most populated conformers of **3AP** in the gaseous phase (**g′GG′g**) and in the liquid phase (**g′G′Gg**) [3]. To name the conformers, we used four letters, the first referring to the configuration around the C–N bond, the second and the third to the configurations around the C–C bonds and the fourth to the configuration around the C–O bond. The letters g/G, g′/G′ and t/T indicate dihedral angles close to 60, −60 and 180°, respectively.

the compound is very hygroscopic, it was stored and manipulated under nitrogen atmosphere to avoid contact with air.

DSC experiments were carried out between 27 and −150 °C. Thermograms were obtained with a Perkin–Elmer DSC_7 apparatus controlled with the *Pyris* Software [12] and operated in the low temperature mode using liquid N_2 as refrigerator. The calibration of the calorimeter for temperatures and heat flows was made from the melting of ice from deionized water ($T_m = 0$ °C and $\Delta H = 333.8$ J g^{-1}) and the crystallographic transition of cyclohexane ($T = -87.1$ °C) at a warming rate of 2.5 °C min^{-1} after quenching. **3AP** samples of a few milligrams (between 2 and 5 mg) were studied in different cooling–warming cycles using cooling and warming rates that varied between 1 and 320 °C min^{-1}. Initially, the experiments were conducted using standard aluminium pans (Perkin–Elmer, 0219-0062) designed for volatile samples. However, the samples were found to react with the container [13] and the analyses were repeated with pans which were covered inside, by sputtering deposition, with 1 μm of gold over a 100 Å layer of tungsten/titanium alloy. This thin layer of gold prevented any chemical reactions to take place. The tungsten/titanium alloy was needed to prevent the gold from peeling off.

The Raman and the powder X-ray experiments were undertaken after the DSC measurements once identified, for each cooling–warming cycle, the relevant phase transition temperatures. The experimental procedure followed in both cases consisted in the simulation of the conditions used in the DSC measurements regarding cooling and warming rates and range of temperatures covered, with registration of spectra (or diffractograms) at a characteristic temperature of each phase detected by DSC.

The X-ray measurements were realized on an Enraf Nonius FR 590 powder diffractometer (Cu Kα_1 radiation, $\lambda = 1.540598$ Å, LFF, 40 mA, 50 kV, curved quartz monochromator) with Debye–Sherrer geometry, equipped with a CPS120 detector and an Enraf Nonius low temperature device (FR558-S). Glass capillaries with a diameter of 0.5 mm were used. The powder diffraction patterns were recorded in transmission mode, over the 2θ range 0–110°. Calibration of the diffractometer was made using potassium aluminate dodecahydrate in a 0.3 mm capillary. The strongest peaks of each powder diffraction pattern were used for automatic indexing using the program *Dicvol91* [14]. The reliability of the powder-pattern indexing solutions found was evaluated using adequate merit figures, as described in [15,16].

Raman spectra were obtained using a Spex 1403 double monochromator spectrometer (focal length 0.85 m, aperture $f/7.8$) equipped with holographic gratings with 180 groove/mm (reference 1800-1SHD). The 514.5 nm Ar^+ laser, adjusted to provide 220 mW power at the sample, was used as excitation radiation. Detection was made using a thermoelectrically cooled Hamamatsu R928 photomultiplier. The sealed glass capillary containing the sample was placed in a Harney–Miller cell, cooled by means of a continuous flux liquid N_2 refrigeration system. This system integrates a solenoid valve (Oxford Instruments), which regulates the N_2 flux that passes through the cell and is controlled by a temperature controller (Red Lion Controls, model T48). The temperature at the sample was measured by a copper/constantan sensor. All the spectra were recorded using increments of 2 cm^{-1} and integration times of 1 s.

3. Results and discussion

3.1. DSC studies

Fig. 2 presents the DSC curves, between 25 and −150 °C, obtained for a sample of **3AP** cooled at cooling rates (ν_c) of 320, 20, 2.5 and 1 °C min^{-1}, and then heated at a constant warming rate (ν_w) of 20 °C min^{-1}.

It is clear from Fig. 2(a)) that quenching of the sample at 320 °C min^{-1} produces a vitreous state, indicating that this cooling rate is fast enough to prevent crystallization of the compound. The thermogram of the subsequent warming shows a step change of the heat capacity, which represents a glass transition (glass transition temperature, $T_g \approx -101$ °C), followed by three additional transitions. The first exothermic, at ca. −75 °C, is associated with the crystallization of the supercooled liquid into a solid form (form **II**), with $\Delta H \approx -9$ kJ mol^{-1}. A second exothermic, with a smaller ΔH

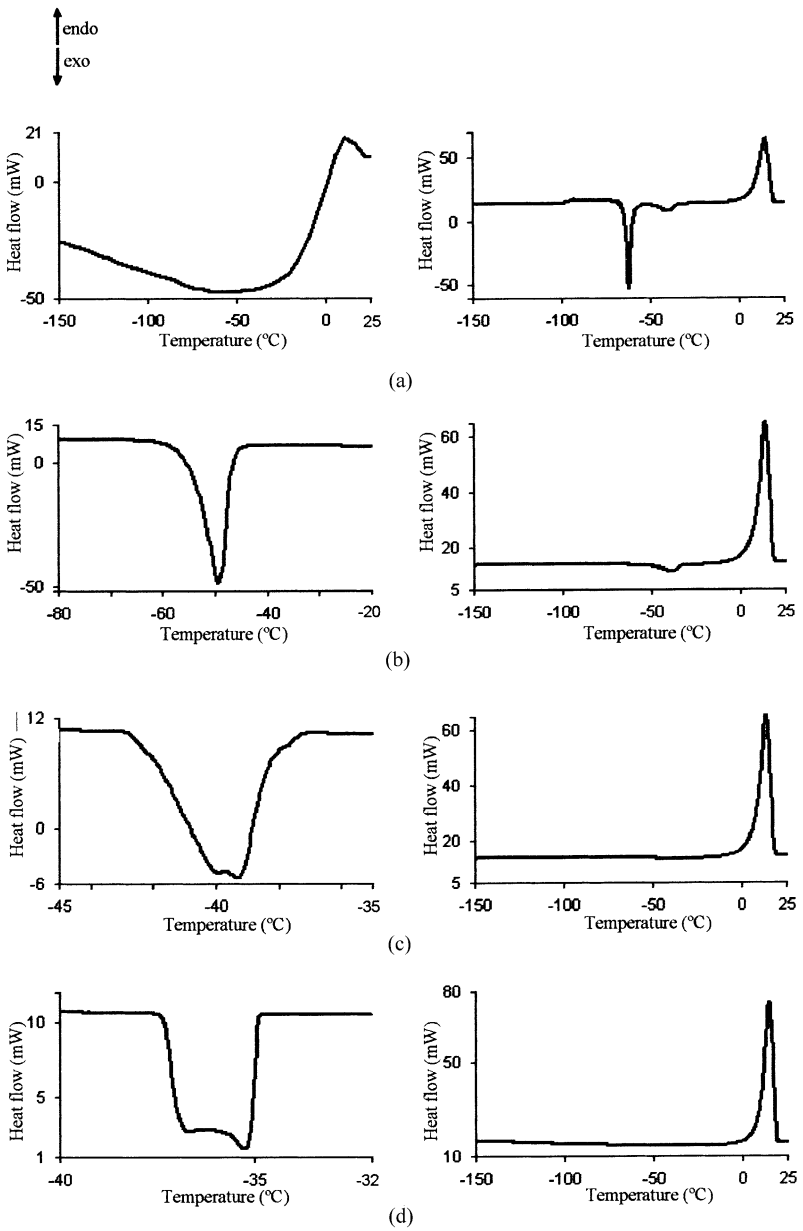

Fig. 2. DSC traces representing the cooling (left side) and re-warming (right side) of **3AP** using different experimental conditions: all warming rates are 20 °C min^{-1}; cooling rates are (a) 320 °C min^{-1}, (b) 20 °C min^{-1}, (c) 2.5 °C min^{-1}, (d) 1 °C min^{-1}.

(ca. −2 kJ mol^{-1}), appears at ca. −55 °C. As it will be shown below, this exothermic corresponds to a solid–solid transformation from the crystalline form **II** to another polymorph (form **I**). The endothermic peak observed at a higher temperature (≈7 °C) represents the melting of this latter form.

The existence of an exothermic peak for the slower cooling rates (Fig. 2(b)–(d); left side), is indicative that crystallization takes place during cooling. Indeed, these cooling rates are sufficiently slow to allow the sample to crystallize completely, since neither the glass transition nor the crystallization peak at ca.

−75 °C are observed during the subsequent warming procedures (Fig. 2(b)–(d); right side). In addition, the warming curves obtained after cooling the sample at 20, 2.5 and 1 °C min^{-1} show the melting peak at the same temperature as that obtained after quenching, indicating that in all cases solid **3AP** was exclusively in the crystalline form **I** before melting. Melting of crystalline form **II** was never observed.

However, a more detailed examination of the thermograms on warming reveals a fundamental difference between the process that takes place during the cooling at 20 °C min^{-1} and those occurring for the slowest cooling rates used (2.5 and 1 °C min^{-1}). The exothermic peak at ca. −55 °C that corresponds to the solid–solid transition (form **II** ⇛ form **I**) is present in the first warming curve (Fig. 2(b); right side), whereas it is absent from the remaining two warming thermograms. Since the melting temperature observed was the same in all cases, being associated with the fusion of the crystalline form **I**, it can be concluded that, contrarily to what happened when the sample was cooled at higher rates, when the 2.5 and 1 °C min^{-1} cooling rates were applied this crystalline variety was formed on cooling. The cooling rates of 2.5 and 1 °C min^{-1} are then slow enough to allow crystallization of form **I** during cooling, whereas cooling the sample at 20 °C min^{-1} is too fast to permit this crystalline variety to be formed and crystal **II** is formed instead.

Another interesting question is if polymorph **I** is directly formed from the liquid state upon cooling at $\nu_c = 2.5$ or 1 °C min^{-1} or if it is formed as the final product of a succession of processes that includes, in first place, formation of polymorph **II** and, after that, its transformation in the solid state into form **I**. The asymmetric shape and broadness of the exothermic peaks obtained on cooling at the two slowest cooling rates (Fig. 2(c) and (d), left side) sustain the second hypothesis.

Polymorphs, or strictly dimorphs where only two forms are under consideration, may be in an enantiotropic or monotropic relationship [10,11]. An enantiotropic relationship implies that each form has a range of temperature over which it is stable with respect to the other and a transition point at which the forms are equistable and in principle interconvertible. In the case of a monotropic relationship, only one polymorph is stable at all temperatures below the melting point, with the other form being therefore unstable over all temperatures. Forms outside their range of stability are usually described as metastable [11]. To decide whether two polymorphs are enantiotropes or monotropes, Burger and Ramberger developed some thermodynamic rules [17] that can be applied to the present system. The 'heat of transition rule' states that, if an endothermic transition between polymorphs is observed, the two forms are enantiotropes. Conversely, if an exothermic polymorphic transition is verified, the forms are monotropes. In the case of the polymorphs of **3AP** the solid–solid transition is exothermic, which means that the relation between the polymorphs is monotropic. Moreover, annealing of the sample around the transition temperature revealed that the observed process is irreversible, further reinforcing the interpretation establishing the monotropic character of the relationship between the two observed polymorphs [17], with **II** being the metastable polymorph and **I** the stable form.

The fact that the formation of the metastable crystal **II** always anticipates the formation of the stable polymorph **I** (as mentioned before, this was observed for **3AP** even when the slowest cooling rates of 2.5 and 1 °C min^{-1} were used) is in consonance with Ostwald's step rule [18], that states that it is not the most stable state with the lowest amount of free energy that is initially formed but the least stable state lying nearest in free energy to the original state.

We have also investigated the effect of applying different warming rates to the sample previously cooled at 320 °C min^{-1}. Whatever the warming rate used between 1 and 80 °C min^{-1} the thermogram obtained was similar to that shown in Fig. 2(a) (right side), i.e. after the glass transition, crystallization of form **II** occurs followed by its transformation into form **I**. Phase transition temperatures obtained for a sample of **3AP** submitted to a warming rate of 2.5 °C min^{-1}, after quenching at 320 °C min^{-1}, are shown in Table 1.

In summary. DSC studies allowed us to verify that within the range of temperatures studied **3AP** may crystallize in two monotropic phases, **I** and **II**, the first being the stable polymorph. A cooling rate of 320 °C min^{-1} is sufficient to produce an amorphous state that, on heating, crystallizes into polymorph **II**. At higher temperatures, this metastable polymorph

Table 1
DSC studies on 3-amino-1-propanol. Phase transition temperatures and enthalpies observed after the glass transition, at $T_{g,1/2} = -100.6 \pm 0.2$ °C with $\Delta C_p = 0.13 \pm 0.04$ kJ mol^{-1} K^{-1}, for $\nu_w = 2.5$ °C min^{-1} after sample's quenching at $\nu_c = 320$ °C min^{-1}

	$T_{o,e}$ (°C)	T_p (°C)	ΔH (kJ mol^{-1})	Phase transition description
1st Exothermic transition	-75 ± 2	-72 ± 2	-8.9 ± 0.2	$Liquid_{supercool} \rightarrow$ crystal solid II
2nd Exothermic transition	-55.3 ± 0.9	-49.4 ± 0.7	-1.94 ± 0.06	Crystal solid II $\rightarrow$ crystal solid I
Endothermic transition	7 ± 1	10.9 ± 0.6	16.9 ± 0.2	Melting: crystal solid I $\rightarrow$ liquid

The results correspond to the average of three tests with the same sample. The uncertainty of the results corresponds to $2s$ (s = standard deviation). $T_{o,e}$ extrapolated onset temperature; T_p peak temperature; ΔH transition enthalpy. The glass transition temperature was determined at half height of the heat capacity variation; all the other phase transition temperatures correspond to the extrapolated onset temperature values.

converts into the stable crystal **I**. For intermediate cooling rates (e.g. 20 °C min^{-1}), **3AP** has time to crystallize as form **II**, the solid **II** $\rightrightarrows$ solid **I** transition occurring during the subsequent heating. A cooling rate of 2.5 °C min^{-1} is slow enough to allow this last process to occur during cooling.

3.2. X-ray powder diffraction and Raman spectroscopic studies

The powder X-ray diffraction and Raman spectroscopy studies undertaken in this work confirmed the results obtained by DSC regarding the different low temperature phases of **3AP** and provided important additional information on their structures at a molecular level.

Three types of powder diffractograms were obtained in the X-ray experiments (Fig. 3). Spectrum (iii) in Fig. 3 was registered at −120 °C (below the glass transition) after quenching **3AP** from the liquid state and it corresponds to the amorphous state. Spectrum (ii) was obtained at −65 °C after re-warming of the glass, and corresponds to the diffractogram of crystal **II**. As expected taking into consideration the DSC data, the same diffractogram was obtained during a moderate cooling ($\nu_c \approx 20$ °C min^{-1}) of the liquid at a temperature of −80 °C (i.e. after the crystallization peak shown in the cooling DSC trace of Fig. 2(b)). When a sample exhibiting a diffractogram characteristic of crystal **II** was heated till −30 °C (temperature above the solid **II** $\rightarrow$ solid **I** transition on warming) a new diffractogram was obtained (spectrum (i) in Fig. 3), that is due to the stable crystal **I**. Also in consonance with the DSC results, a cooling rate of ≈2.5 °C min^{-1} applied to the sample produces the diffraction powder pattern registered at −80 °C, characteristic of form **I** (spectrum (i) in Fig. 3), Moreover, further cooling down till −120 °C as well as subsequent warming till just before melting did not lead to any change in the registered diffractogram.

Comparison of the characteristic diffractograms of the two polymorphs (i) and (ii) in Fig. 3) shows that the diffractogram corresponding to form **II** consists of considerably broader peaks than that associated with form **I**. This fact is indicative of a lower degree of crystalinity of the metastable polymorph when compared with the stable form.

The solutions obtained by powder patterns indexation of forms **II** and **I** belong to the monoclinic system. For the stable form **I**, the indexation procedure produced the solution presented in Table 2, with figures of merit [15,16] $M(25) = 16.3$ and $F(25) = 18.3$, where 25 is the number of diffraction peaks considered for indexation. The crystalline unit cell of polymorph **I** has four molecules and a volume, V, of 432.52 Å^3. The reflections hkl obey to the condition $h + k = 2n$ (n an integer) and those of the type $h0l$ have $l = 2n$ and $h = 2n$; it was also indexed one reflection of the type $0K0$ with $K = 2n$. These conditions point out [19] to one of the possible space symmetry groups: $C2$, Cm or Cc (thus, the number of molecules in the primitive cell will be half the number existent in the unit cell, i.e. 2).

For the metastable form **II**, indexation of its powder diffraction pattern led to a number of different possible solutions in the monoclinic system, all of them with similar merit figures; thus, it was impossible to uniquely determine which represents the true solution. In order to characterize this phase

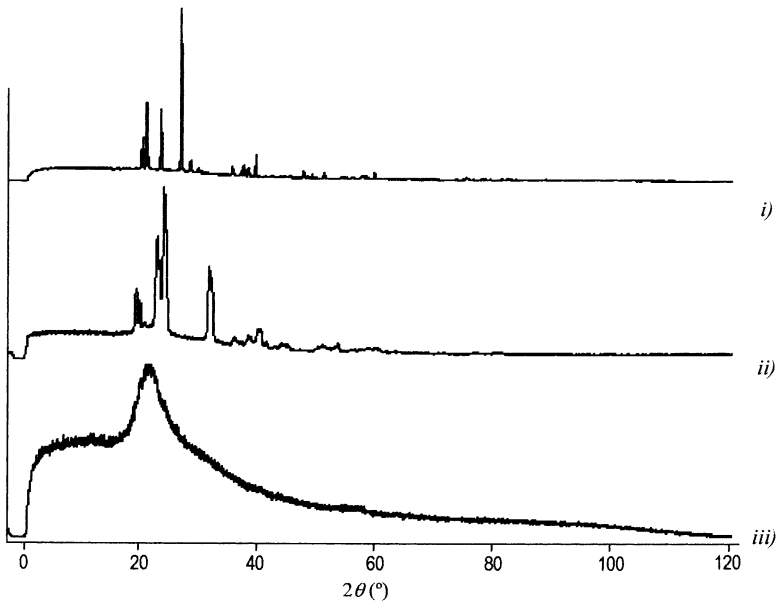

Fig. 3. Observed powder X-ray diffractograms of **3AP** in (i) crystalline polymorph **I**, (ii) crystalline polymorph **II** and (iii) low temperature amorphous state.

(and also to obtain additionally structural information about crystal **I**) single crystal X-ray measurements appear to be fundamental. However, since **3AP** is liquid at room temperature (and also a hygroscopic substance), to obtain suitable single crystals for these studies is particularly challenging and requires specialized know-how and experimental conditions that are not available in our laboratories [20].

In the Raman studies, three types of spectra were also observed during the experiments, which correspond to the spectral signatures of the two crystalline states and amorphous phase. Spectrum (iii) in Fig. 4 was obtained after fast cooling of liquid **3AP** from room temperature to −120 °C and corresponds to the amorphous solid. As expected, this spectrum is identical to the Raman spectrum of the pure liquid at room temperature [3,6]. The characteristic Raman spectra of crystalline states **I** and **II** are shown in Fig. 4(i) and (ii). These spectra shown in this figure were collected at −40 and −5 °C, respectively, within the expected temperature ranges for observation, under favorable conditions, of each crystalline form. Indeed, the experimental cooling and warming rates used and the temperatures for spectra collection were identical

Table 2
Cell unitary parameters of crystalline stable form **I** of 3-amino-1-propanol at low temperatures

[a]	Crystalline form **I**[b,c]
System	Monoclinic
Space symmetry group	*C*2, *Cm* ou *Cc*
a (Å)	5.945 ± 0.002
b (Å)	8.403 ± 0.003
c (Å)	8.678 ± 0.003
β (°)	93.85 ± 0.03
V (Å^3)	432.52
Z	4
Z′	2

[a] Abbreviation: *a*, *b* e *c*: modulus of the vectors $\vec{a}$, $\vec{b}$ and $\vec{c}$ that generate the unitary cell; *β* angle between $\vec{a}$ and $\vec{c}$; *V* unitary cell volume; *Z* number of molecules in the unitary cell; *Z*′ number of molecules in the primitive cell.

[b] The parameters were determined by powder pattern indexation by means of *Dicvol91* [14]. The indexation of 25 peaks conducted to the presented solution with merit figures $M(25) = 16.3$ e $F(25) = 18.3$.

[c] The results uncertainty corresponds to *s* (*s* = standard deviation).

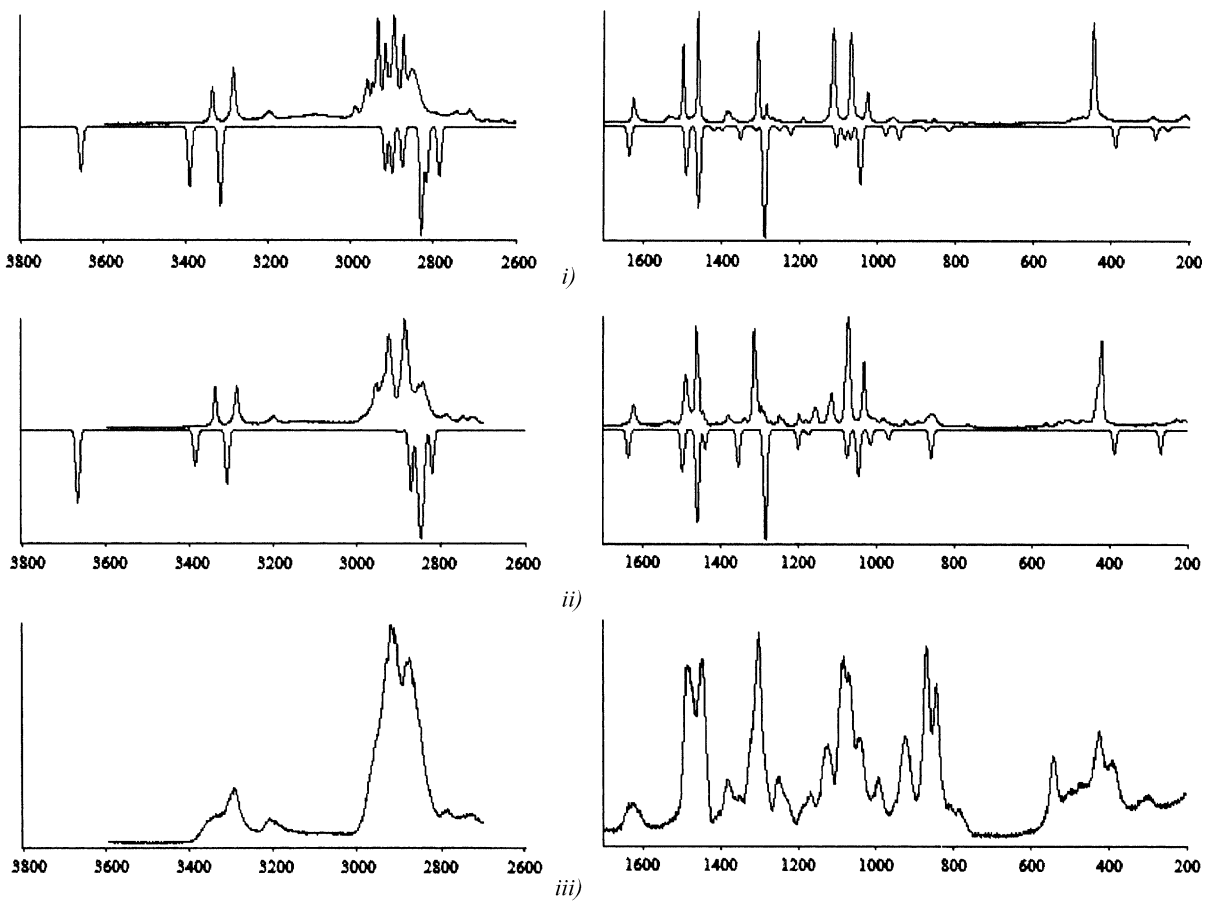

Fig. 4. Spectra pointing up: observed Raman spectra of **3AP** in (i) crystalline polymorph **I**, (ii) crystalline polymorph **II** and (iii) low temperature amorphous state. Spectra pointing down: HF/6-31G* (scaled) calculated Raman spectra for (i) conformer **gTTg** and (ii) conformer **tTTt** of **3AP**.

to those used to obtain the characteristic diffractograms of the two polymorphs in the powder X-ray diffraction experiments; the observed temperature ranges for existence of each crystalline form were also found to be nearly the same in both kinds of experiments.

The conversion of one polymorph into another is accompanied by a structural reorganization at a molecular level. Any change of packing will cause geometrical changes in the molecules and, conversely, any generalized change in the geometry of the molecules within a crystal will invite different packing. The extent of the structural reorganization will depend on the structural flexibility of the molecules. **3AP** is a flexible molecule, exhibiting 38 conformational states of relatively low energy, as predicted by previous ab initio studies on this molecule [3,6]. Therefore, the solid–solid transformation from crystal **II** into crystal **I** shall be accompanied by a conformational change in the individual molecules.

To shed light on the conformations adopted by the **3AP** molecules in each polymorph, we performed a systematic comparison of the observed Raman spectra with those predicted theoretically for each one of the 38 conformers of **3AP** [3,6]. This approach assumes that the identity of each molecular conformation is essentially preserved in the crystal structures and requires that some easily predictable spectral changes due to intermolecular interactions be taken into consideration during the analysis of the data (e.g. OH···N and NH···O intermolecular hydrogen

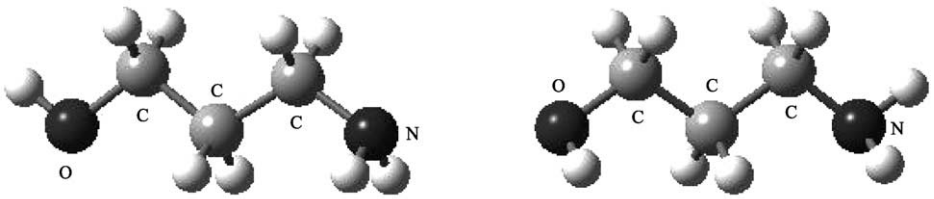

Fig. 5. Conformers **tTTt** and **gTTg** of **3AP**.

bonding leads to well known shifts in the frequencies of the νOH and νNH stretching vibrations—which decrease—and τHOCC, τCCNH torsions—which increase [3,6]).

Among the 38 conformers of **3AP**, those exhibiting a *gauche* configuration of the NCCC or CCCO axes give rise to a Raman spectra with a profile, in the region 1600–600 cm^{-1}, that is markedly different from the experimental spectra of the crystalline states. Only 5 conformers have both NCCC and CCCO axes in the *trans* configuration (**tTTg**, **g′TTg**, **gTTg**, **gTTt** and **tTTt**) and these were considered for further investigation. Note that a *trans* configuration around the central bonds implies that the OH and NH_2 groups are kept as much apart as possible from each other, making more difficult the establishment of intramolecular hydrogen bonds and facilitating the participation of these groups in intermolecular hydrogen bonding. In spite of the relative similarity of the spectra predicted for the 5 conformers with *trans* NCCC and CCCO axes, those belonging to conformers **gTTg** and **tTTt** (shown in Fig. 5) were found to fit better the experimental data for crystal **I** and **II**, respectively.

Simulated (HF/6-31G* [6]) Raman spectra of conformers **gTTg** and **tTTt** are compared with the experimental spectra of crystalline polymorphs **I** and **II** in Fig. 4(i) and (ii), respectively. The assignment of the observed bands, presented in Tables 3 and 4 for the two crystals, was made taking into consideration those theoretical spectra.

The spectra of the two crystalline varieties are particularly different in the νCH_2 region. The observed differences were well predicted by the calculated spectra. For conformer **tTTt**, the six vibrational modes expected in this region

Table 3
Comparison of Raman spectrum of crystal **II** with the calculated HF/6-31G* spectrum of conformer **tTTt**

Exp.		HF/6-31G* **tTTt** [6]		Assignment[a]
ν	I^a	ν	I^R	
3338	S	3385	56.2	νNH_2as.
3287	S	3310	84.1	νNH_2s.
3198	m	3665	116.7	νOH
2954	S	2898	3.7	νCH_2as.′
2924	vS	2872	97.3	νCH_2as.″
2924	vS	2856	57.0	νCH_2s.″
2886	vS	2849	133.7	νCH_2s.′
2886	vS	2842	91.8	νCH_2as.
2843	S	2821	68.2	νCH_2s.
2788	w			Comb.[b]
2748	w			Comb.[c]
2723	w			Comb.[d]
1623	m	1637	6.5	δNH_2
1535	w			Comb.[e]
1490	S	1498	9.1	δCH_2
1470	vw	1469	0.03	δCH_2″
1462	vS	1459	20.7	δCH_2′
1445	m	1439	4.6	ωCH_2
1410	vw	1378	0.1	ωCH_2″
1381	m	1354	8.0	$twCH_2$″
1338	w	1288	1.4	ωCH_2′
1314	vS	1284	23.4	$twCH_2$′
1296	m	1261	0.6	$twCH_2$
1249[f]	m	1200	4.8	δCOH
1241	s			
1198[f]	m	1174	1.7	γCH_2
1180	w			
1155[f]	m	1074	6.5	νCO
1114	m			
1071	vS	1045	10.6	νCN
1031	S	1015	3.9	νCCs.
981	w	992	0.5	γNH_2
923	w	968	2.1	νCcas.
891	vw	825	0.1	γCH_2″

(*continued on next page*)

Table 3 (*continued*)

Exp.		HF/6-31G* **tTTt** [6]		Assignment[a]
ν	I^a	ν	I^R	
858	m	858	6.0	ωNH_2
765	vw	722	0.04	$\gamma CH_2'$
531[f]	w	437	0.2	δCCO
508	w			
473	w	386	5.8	δCCN
430[f]	s	268	5.6	$\tau HOCC$
421	vS			
284	vw	274	0.9	$\tau CCNH$

Wavenumbers (ν) em cm^{-1}; calculated wavenumbers, obtained in [21] at the Hartree–Fock level of theory using the standard 6-31G* split valence basis set with the Gaussian 98 program package [22], were scaled by 0.89 [21]. Raman experimental intensities presented as qualitative relative intensities; Raman calculated HF/6-31G* intensities in km mol^{-1}.

[a] Abbreviations: ν stretching; δ bending; ω wagging; tw twisting; γ rocking; τ torsion; as. asymmetric; s. symmetric. comb. Combination tone; S strong; vS very strong; m medium; w weak; vw very weak; s shoulder.

[b] $\delta CH_2'' + twCH_2'$ combination.

[c] $\delta CH_2' + twCH_2$ combination.

[d] $\delta CH_2 + \delta COH$ combination.

[e] $\nu CO + \tau HOCC$ combination.

[f] Crystal field splitting.

Table 4
Comparison of Raman spectrum of crystal **I** with the calculated HF/6-31G* spectrum of conformer **gTTg**

Exp.		HF/6-31G* **gTTg** [6]		Assignment[a]
ν	I^a	ν	I^R	
3335	S	3390	79.7	νNH_2as.
3284	S	3316	105.5	νNH_2s.
3197	m	3653	60.9	νOH
2961	S	2916	58.1	νCH_2as.
2948[b]	m	2900	61.9	νCH_2as.′
2936	vS			
2917	S	2875	53.0	νCH_2as.″
2897	vS	2829	145.4	νCH_2s.
2874	vS	2816	73.1	νCH_2s.′
2853	S	2785	66.5	νCH_2s.″
2744	w			comb.[c]
1624	m	1636	7.0	δNH_2
1534	w			Comb.[d]
1500	vS	1491	12.9	δCH_2
1500	vS	1481	0.3	$\delta CH_2''$
1462	vS	1460	20.5	$\delta CH_2'$
1387	m	1352	3.6	δCOH

Table 4 (*continued*)

Exp.		HF/6-31G* **gTTg** [6]		Assignment[a]
ν	I^a	ν	I^R	
1366	w	1420	1.3	$\omega CH_2''$
1366	w	1400	1.6	ωCH_2
1307	vS	1289	27.1	$twCH_2'$
1307	vS	1312	1.8	$twCH_2''$
1285	m	1224	2.6	$\omega CH_2'$
1269	vw	1253	1.4	γCH_2
1190	w	1106	5.7	γNH_2
1113	vS	1069	3.1	νCO
1113	vS	1085	3.6	$twCH_2$
1068	vS	1044	14.6	νCN
1026	m	980	2.8	$\nu CCs.$
961	w	945	3.7	$\nu CCas.$
892	w	877	1.7	ωNH_2
855	w	817	1.9	$\gamma CH_2''$
763	vw	730	0.3	$\gamma CH_2'$
503	vw	443	0.4	δCCN
446	vS	287	3.5	$\tau HOCC$
417	vw	390	5.1	δCCC
295	w	256	1.1	$\tau CCNH$
211	w	183	0.4	δCCO

Wavenumbers (ν) em cm^{-1}; calculated wavenumbers, obtained in [21] at the Hartree–Fock level of theory using the standard 6-31G* split valence basis set with the Gaussian 98 program package [22], were scaled by 0.89 [21]. Raman experimental intensities presented as qualitative relative intensities; Raman calculated HF/6-31G* intensities in km mol^{-1}.

[a] Abbreviations: ν stretching; δ bending; ω wagging; tw twisting; γ rocking; τ torsion; as. asymmetric; s. symmetric. comb. Combination tone; S strong; vS very strong; m medium; w weak; vw very weak; s shoulder.

[b] Crystal field splitting.

[c] $\delta CH_2' + \omega CH_2'$ combination.

[d] $\nu CO + \tau HOCC$ combination.

(2700–2900 cm^{-1}) were predicted to have relatively close frequencies; accordingly, in this region, the observed spectra of crystal **II** shows only four bands. In contrast, the predicted frequencies for the same modes in the **gTTg** conformer are well separated and, in agreement with this prediction, six bands are observed in the Raman spectra of crystal **I**. The calculations also predict fairly well the position of the most intense bands in the spectra of the two polymorphs: $\tau HOCC$, νCN, $twCH_2'$ and $\delta CH_2'$ for crystal **II**, and νCO, $twCH_2$, δCH_2 and $\delta CH_2''$ for crystal **I** (see Tables 3 and 4 and Fig. 4).

In summary. Powder X-ray diffraction and Raman experiments confirm the results obtained by DSC regarding the low temperature phases of **3AP** and the required conditions to produce each one of them. Besides, the two crystalline monotropic polymorphs were structurally characterized at a molecular level. In particular, the spectroscopic data indicates that different conformations are assumed by the individual molecules of **3AP** in the two crystalline varieties. Taking into consideration the comparison between the observed and the theoretically predicted Raman spectra, the **tTTt** and **gTTg** conformers are here tentatively assigned as the conformers existing in the crystalline phases **II** and **I**, respectively.

Acknowledgements

The authors would like to thank E. Andre for his help concerning the sputtered gold plating of the aluminium pans and Dr. J. Cecílio for the help concerning the Raman experiments. This study is partially supported by the Fundação para a Ciência e a Tecnologia (FCT), Lisbon (research projects POCTI/43366/QUI/2001 and POCTI/33495/QUI/2000. PhD Grant GGPXXI/BD/3873/96).

References

[1] A. Baudot, C. Cacela, M.L. Duarte, R. Fausto, Cryobiology 44 (2002) 150.
[2] C.F. Cacela, P. da Silva, M.L. Duarte, R. Fausto, J. Mol. Struct. 482–483 (1999) 591.
[3] C. Cacela, M.L. Duarte, R. Fausto, Spectrochim. Acta A 56 (2000) 1051.
[4] R. Fausto, C. Cacela, M.L. Duarte, J. Mol. Struct. 550–551 (2000) 365.
[5] C. Cacela, R. Fausto, M.L. Duarte, Vibrat. Spectrosc. 26 (2001) 113.
[6] C. Cacela, PhD Thesis, Faculdade de Ciências da Universidade de Lisboa, 2002.
[7] M.A. McMahan, S.D. Sharma, R.F. Curl Jr., J. Mol. Spectrosc. 75 (1979) 220.
[8] K. Iijima, T. Unno, J. Mol. Struct. 445 (1998) 179.
[9] J.D. Dunitz, Pure Appl. Chem. 63 (1991) 177.
[10] D.J.W. Grant, in: H.G. Brittain (Ed.), Drugs and the Pharmaceutical Sciences—Polymorphism in Pharmaceutical Solids, Vol. 95, Marcel Dekker, Inc, New York, 1999, p. 1.
[11] T.L. Threlfall, Analyst 120 (1995) 2435.
[12] PYRIS software for windows (version 3.72), copyright © 1996–1999 Perkin Elmer LLC.
[13] R.E. Lenga, The Sigma-Aldrich Library of Chemical Safety Data, 1st ed., Sigma Aldrich Corporation, Milwaukee WI, 1986, p. 863.
[14] A. Boultif, D. Louër, J. Appl. Crystallogr. 24 (1991) 987.
[15] G.S. Smith, R.L. Snyder, J. Appl. Crystallogr. 12 (1979) 60.
[16] P. De Wolff, J. Appl. Crystallogr. 24 (1991) 987.
[17] A. Burger, R. Ramberger, Mikrochim. Acta II (1979) 259.
[18] W. Ostwald, Z. Physik. Chem. 22 (1897) 289.
[19] N.F.M. Henry, K. Lonsdale (Eds.), International Tables for X-ray Crystallography, Vol. 1, Kynoch Press, Birmingham, 1952.
[20] D. Brodalla, D. Mootz, R. Boese, W. Osswald, J. Appl. Crystallogr. 18 (1985) 316.
[21] D.J. Defrees, A.D. McLean, J. Chem. Phys. 82 (1985) 333.
[22] M.J. Frisch, G.W. Trucks, H.B. Schlegel, G.E. Scuseria, M.A. Robb, J.R. Cheeseman, V.G. Zakrzewski, J.A. Montgomery, R.E. Stratmann, J.C. Burant, S. Dapprich, J.M. Millam, A.D. Daniels, K.N. Kudin, M.C. Strain, O. Farkas, J. Tomasi, V. Barone, M. Cossi, R. Cammi, B. Mennucci, C. Pomelli, C. Adamo, S. Clifford, J. Ochterski, G.A. Petersson, P.Y. Ayala, Q. Cui, K. Morokuma, D.K. Malick, A.D. Rabuck, K. Raghavachari, J.B. Foresman, J. Cioslowski, J.V. Ortiz, B.B. Stefanov, G. Liu, A. Liashenko, P. Piskorz, I. Komaromi, R. Gomperts, R.L. Martin, D.J. Fox, T. Keith, M.A. Al-Laham, C.Y. Peng, A. Nanayakkara, C. Gonzalez, M. Challacombe, P.M.W. Gill, B.G. Johnson, W. Chen, M.W. Wong, J.L. Andres, M. Head-Gordon, E.S. Replogle and J.A. Pople, Gaussian 98 (Revision A.9), Gaussian, Inc., Pittsburgh PA, 1998.